

On the experimental feasibility of quantum state reconstruction via machine learning

Sanjaya Lohani^{1,*}, Thomas A. Searles^{2,3}, Brian T. Kirby^{1,4,+}, and Ryan T. Glasser^{1,++}

¹Tulane University, New Orleans, LA 70118, USA

²Massachusetts Institute of Technology, Cambridge, MA 02139, USA

³Howard University, Washington, DC 20059, USA

⁴United States Army Research Laboratory, Adelphi, MD 20783, USA

*slohani@tulane.edu

+brian.t.kirby4.civ@mail.mil

++rglasser@tulane.edu

ABSTRACT

We determine the resource scaling of machine learning-based quantum state reconstruction methods, in terms of both inference and training, for systems of up to four qubits. Further, we examine system performance in the low-count regime, likely to be encountered in the tomography of high-dimensional systems. Finally, we implement our quantum state reconstruction method on a IBM Q quantum computer and confirm our results.

Main

Quantum state tomography is a standard procedure for reconstructing the state of an unknown quantum system through a series of repeated measurements on an ensemble of identically prepared systems. The number of measurement settings required for full state tomography of a multi-qubit state scales exponentially with the qubit number¹. Further, the determination of a physically valid density matrix that corresponds to the measured data is itself resource-intensive^{2,3}. Many methods for reconstructing valid density matrices from measured data have been developed, such as Bayesian⁴, maximum likelihood estimation (MLE)^{3,5,6}, projected gradient descent⁷, and linear regression⁸. Recently, several methods for state reconstruction based on machine learning have been proposed and demonstrated⁹⁻¹⁵. These machine learning-based techniques offer several potential advantages compared to their conventional counterparts, such as the ability to front-load expensive computations and robustness to missing measurements and experimental noise¹⁶. Despite these advantages, it is not yet clear how the machine learning models' training scales with system size, nor how they perform in situations where limited copies of the unknown state are available.

In this brief communication, we implement quantum state tomography for systems of up to four qubits on the IBM Q quantum processor and reconstruct the measured states via a neural network. In all cases, we either match or exceed the fidelities achieved compared to MLE. Using our results, we can estimate the resource scaling of both training and inference for our system. Further, we investigate the impact of statistical noise on our neural network system by limiting how many copies of an unknown state are available for tomographic measurements. We find that when performing state reconstruction on data obtained from only a few copies of a state, meaning significant statistical noise is present in the measurement results, we obtain enhanced reconstruction fidelity by using training data that includes comparable statistical noise. In other words, the variations in measurement results due to limited counting statistics are themselves learnable, to some degree, by our network. These results inform the applicability of neural network quantum state reconstruction for high-dimensional systems where resource limitations in computation and the repeatability of measurements are important factors.

An end-to-end tomography setup with a neural network is shown in Fig. 1 (a). First, we make predictions for unknown test quantum states with a network solely trained with ideal, simulated tomography data (see “Methods”), the results of which are shown in Fig. 1 (b, c). With the trained network, the fidelity between the reconstructed and corresponding target density matrices systems of one, two, three, and four qubits are shown in Fig. 1 (b). The reconstruction fidelity per epoch for the random quantum states from the validation set in the cases of one and four qubits are shown in the inset. We implement the network using tensorflow¹⁷ with an AMD Ryzen 9 3900x 12-core processor and GeForce RTX 2060 GPU. We find that the network takes only 14 seconds for a single qubit, and 240 seconds for four qubits in order to reach saturation. The red, blue, and green lines respectively represent the fidelity for the test set from the ideal scenario, the IBM Q simulator with noise, and

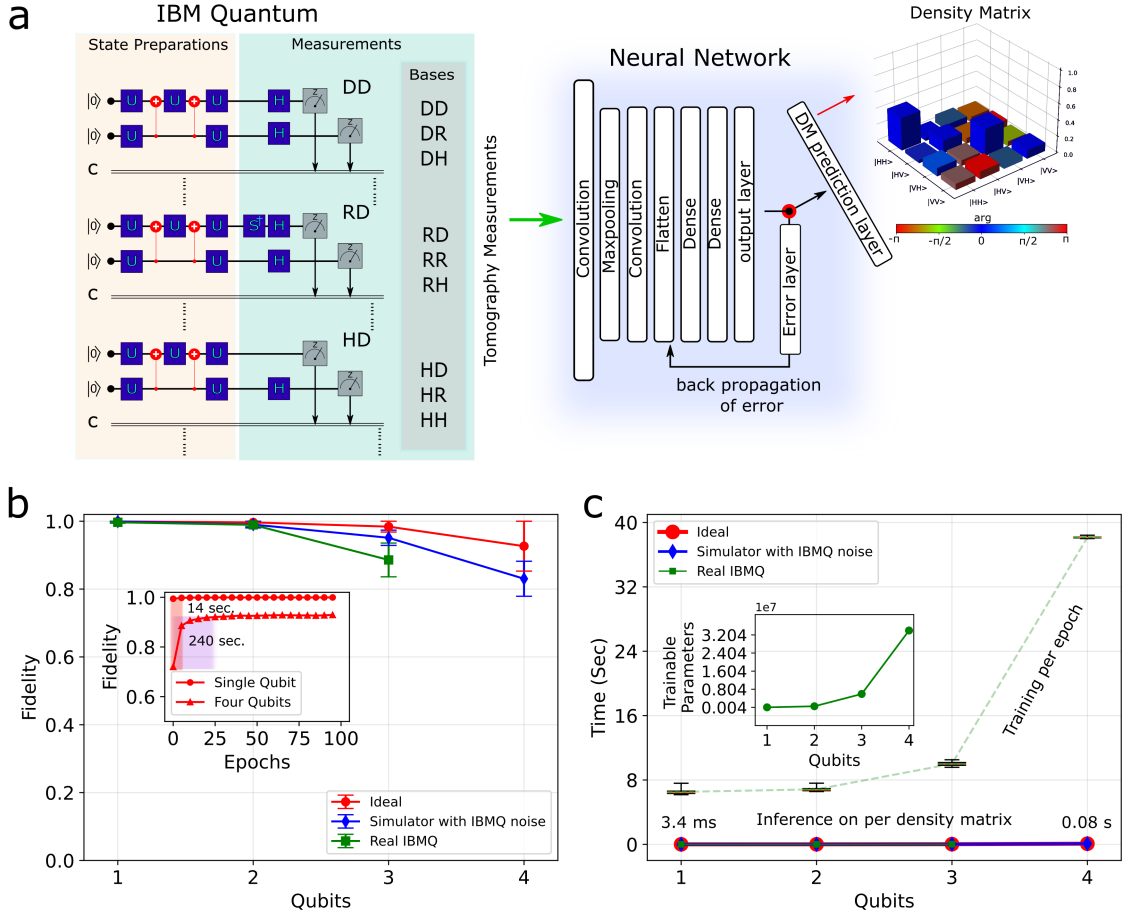


Figure 1. Network architecture and reconstructing quantum states for various sizes of qubits. (a) Example of an end-to-end tomography setup with a qubit size of two. Abbreviations H, D, and R, respectively represents horizontal, diagonal and right-circular polarization basis. The density matrices (DM) are predicted at the DM prediction layer. (b) Fidelity for the predicted density matrices versus the number of qubits. The error bars show one standard deviation from the mean. The inset shows the cross-validation fidelity for the ideal test set. (c) Network inferences versus the number of qubits. The whiskers on the box-plot represent fidelity from 1 to 99 percentiles.

the real IBM Q device as described in ‘‘Methods’’. For all the test cases and systems with qubits of size of one and two, we find the trained networks reconstruct the quantum states with near-unity fidelity. Additionally, we find a significant increase in size of the quantum circuit as well as number of gates for higher values of the qubits (see ‘‘Supplementary Fig. S1’’). Consequently, noise in the tomography data from the real IBM Q machine also increases. This results in a decrease in the average fidelity for the three and four qubit cases. Even with such noisy tomography values from the real IBM device, we show that the network trained with ideal tomography sets reconstructs random quantum states of size of three qubits with an average fidelity of 0.89. Examples of the target and predicted density matrices for a qubit size of three are shown in ‘‘Supplementary Fig. S2’’ . Similarly, for a qubit size of four, random quantum states are reconstructed from the tomography data obtained from the IBM Q simulator containing noise with an average fidelity of 0.83. Note that the IBM Q backend transpiles a huge circuit for a qubit size of four as illustrated in ‘‘Supplementary Fig. S1’’ . As a result, we end up with extremely noisy tomography data with the real IBM Q for a qubit size of four.

Next, we evaluate the computational cost on training and testing of the network. As the number of qubits, ‘ d ’, increases, the number of quantum circuits and over-complete tomography values are, respectively, increased on the order of 3^d and 6^d . Because of this we increase the network training parameters accordingly in order to achieve similar fidelities for systems of all qubit sizes. The average training time per epoch versus number of qubits is shown by the green dotted line in Fig. 1 (c). The box plots represent the statistics of the time per epoch from 1 to 99 percentiles. As expected we find that the training time increases with the number of qubits. The sudden rise in the training time for qubit size of four is due to drastic increase in the trainable parameters as illustrated in the inset. However, once the network is trained, we find that the network makes the

prediction of a density matrix for the qubit size of one, and four, respectively, within 3.4 milliseconds and 0.08 seconds. The inference on a density matrix reconstruction for data obtained from the ideal, IBM Q simulator with noise, and real IBM Q hardware cases are, respectively, shown by a red, blue and green solid line in Fig. 1 (c).

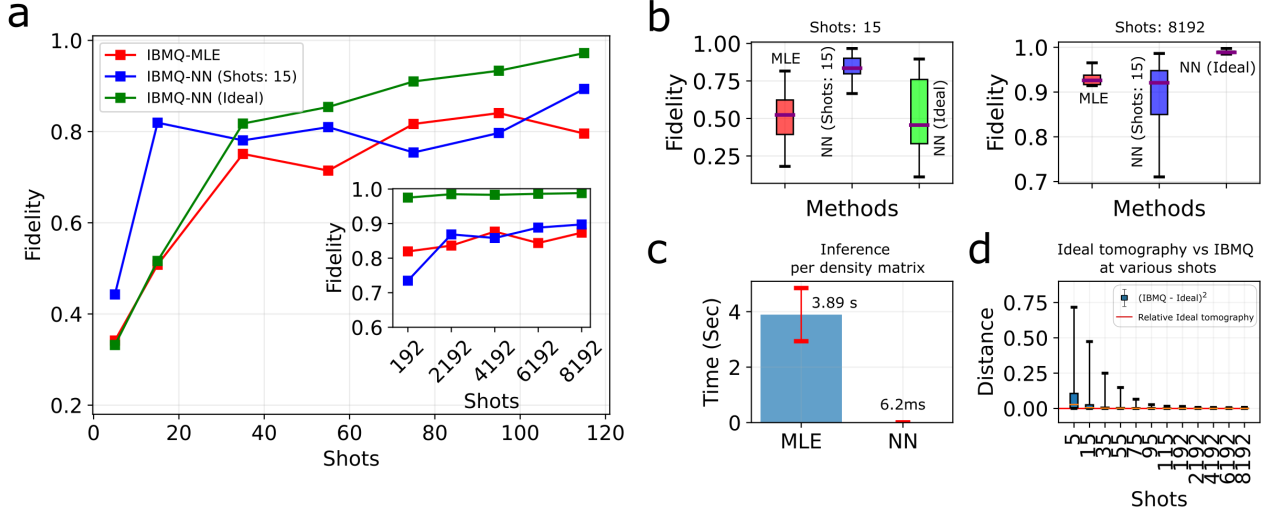


Figure 2. Network performance with varying shots. (a) Reconstruction fidelity for ranges of shots. For larger shots, the fidelity with the networks, and maximum likelihood estimation (MLE) are shown in the inset. (b) Reconstruction statistics at shots 15 (left), and 8192 shots (right). The whiskers on the box-plots represent fidelities from $Q_1 - 1.5(Q_3 - Q_1)$ to $Q_3 + 1.5(Q_3 - Q_1)$, where Q_1 and Q_3 represent the first quartile and third quartile of the fidelity values. (c) Inference on maximum likelihood estimation method, and the trained network. The error bar shows one standard deviation from the mean. (d) Squared differences between the ideal tomography and tomography measured from the real IBM Q computer at various shots.

We now turn to investigating the reconstruction fidelity at various shots, which represents the number of times the same quantum circuit is executed. In order to illustrate the proof of concept, we fix the qubit size at two and vary the number of shots when using different reconstruction methods. Here we implement three methods: a network trained with ideal tomography values “NN (Ideal)”, a network trained with the tomography values simulated at 15 shots “NN (Shots: 15)”, and finally the maximum likelihood estimation (MLE). For each method, experimental shots ranging from 5 to 8192 were executed in order to make predictions for a test set containing tomography data for 20 random quantum states from the real IBM Q computer. The average reconstructed fidelity at various shots is shown in Fig. 2 (a). Moreover, the fidelity at higher shots is shown in the inset. As expected, we find that the network trained with ideal tomography (green line) works better and reaches a fidelity of 0.99 at 8192 shots. Additionally, we show the fidelity at 5 and 15 shots are enhanced with the network that is trained with the simulated data at 15 shots (a blue line). Furthermore, in order to illustrate the performance efficacy of the networks, we also reconstruct random quantum states from the same test-set with MLE as shown by a red line. The statistics of the fidelity for the predicted density matrices at shots 15 (left) and 8192 (right) are shown as the box plots in Fig. 2 (b). We find that the networks trained with ideal tomography and simulated tomography simply outperform MLE. And notably, the network trained for simulated tomography at 15 shots produces higher average fidelity than MLE in lower shots regime.

Similarly, we also make an inference on per density matrix prediction with the MLE and the neural network. We find a significant improvement in computational cost with the network, which is 6.2 milliseconds, compared to MLE, which takes 3.89 seconds, as shown in Fig. 2 (c). The error-bar represents a standard deviation from the mean. Finally, we show the extent of statistical noise as a squared difference between the tomography values from the real IBM Q device and the ideal measurement scenarios at various shots in Fig. 2 (d). As expected, we find noise on the tomography from real IBM Q computer decreases with increasing shots.

In conclusion, we have experimentally investigated the resource and computation time scaling of quantum state tomography using machine learning techniques. We implement quantum state tomography on random quantum states using the IBM Q quantum computer for systems of up to four qubits. We also implement MLE for state estimation and find our neural network system outperforms it in several scenarios. We show that the neural network approach may be useful in larger dimensional systems since the number of repeated circuits necessary for accurate tomographic reconstruction is small. Lastly, we reiterate that while a neural network’s training time increases for quantum systems of increasing dimension, the network need only be trained a single time. Once trained, the inference time when using the neural network in practice is negligible. As such,

the results provide evidence for machine learning as a tool for full quantum state tomography in near-term intermediate-scale quantum hardware.

Methods

Generating random quantum states and measuring the tomography

The random pure quantum states, corresponding density matrices (ρ), and τ vectors, arrays of elements of the lower triangular matrices obtained after applying the Cholesky decomposition to the density matrices¹⁸, are generated as described in¹³. In order to have the ideal tomography set, we apply the relation given by

$$\text{Measurements } (m) = \text{Tr}(\rho \hat{\mathcal{P}}), \quad (1)$$

where ‘Tr’ represents the trace, and $\hat{\mathcal{P}}$ is the set of projectors for the given size of the qubits. Similarly, for the tomography from the IBM Q-qasm simulator with noise and the real IBM Q computer, we first initialize the qubits with the given random quantum states and allow the system to self-optimize the quantum circuits¹⁹. Note that we perform the light order of optimization on the circuits with ‘qiskit.execute’ from the Qiskit Terra API²⁰.

Training the network

We custom build a convolutional neural network with a convolutional unit followed by a max-pooling layer and a second convolutional unit in a row. After that we connect two dense layers each followed by a dropout layer, which is finally attached to an output layer where density matrices are predicted as shown in Fig. 1 (a). First, In order to train the network, we simulate 35,500 random quantum states using the Haar measure and their tomography measurements for systems with number of qubits ranging from one to four. The simulated data are then split into a training set containing 35,000 tomography measurements, and a validation set with 500 tomography measurements to cross-validate the network performance. Additionally, so as to reduce the bias-variance trade-off and increase the fidelity at the output, we use separate networks with different hyper-parameters for different sizes of qubits. Note that we implement the batch size of four in the training of all the networks. Once the networks are trained with simulated data, we then generate test sets which are completely unknown to the trained network. For the test-sets we consider three scenarios, a simulated test-set without any noise (“Ideal”), a test-set generated from the ibmq-qasm-simulator at shots of 2192 with a noise model provided by IBM Q-backend ‘ibmq_rome’ (“Simulator with IBMQ noise”), and finally, a test set containing the tomography data directly measured from the real IBM Q computer (5 qubits machine: *ibmq_rome*). Note that each test set consists of tomography measurements for 20 random quantum states, again for each of the systems from one to four qubits.

Moreover, our custom built network makes the predictions for the τ arrays at the error layer as shown in Fig. 1 (a), which are finally compared with the target τ arrays and the mean squared loss (MSE) is evaluated and finally optimized with the Adagrad optimizer. Also, note that there are no training parameters between the error layer and the density matrix (DM) prediction layer. We build the DM prediction layer in the same graph of the network in order to efficiently evaluate the fidelity metric per epoch to cross-validate the training as well as avoid the post-processing.

Maximum likelihood estimation

For the two qubit case, the over-complete tomography measurement consists of 36 data points m_i , where i runs from 1 to 36. The expected value is assumed to be \bar{m}_i . For simplicity we assume the noise on the tomography is Gaussian, which leads the probability (P) of obtaining a tomography set of m_i to,

$$P(m_1, m_2, \dots, m_{36}) = \prod_{i=1}^{36} \exp \frac{-(m_i - \bar{m}_i)^2}{2\sigma_i^2}. \quad (2)$$

Here σ_i is approximated as $\sqrt{\bar{m}_i}$. As in eqn (1), the expected tomography for the density matrix $\rho(\tau_1, \tau_2, \dots, \tau_{16})$ is

$$\bar{m}_i = \text{Tr}(\rho(\tau_1, \tau_2, \dots, \tau_{16}) \hat{\mathcal{P}}_i). \quad (3)$$

Thus, the negative log-likelihood of the given density matrix $\rho(\tau_1, \tau_2, \dots, \tau_{16})$ that results m_i measurements is

$$-\mathcal{L} = \sum_{i=1}^{36} \frac{\left[\text{Tr}[\rho(\tau_1, \tau_2, \dots, \tau_{16}) \hat{\mathcal{P}}_i] - m_i \right]^2}{2\text{Tr}[\rho(\tau_1, \tau_2, \dots, \tau_{16}) \hat{\mathcal{P}}_i]}. \quad (4)$$

In order to maximize the likelihood, we minimize the right-hand side of eqn (4) using the Broyden–Fletcher–Goldfarb–Shanno (BFGS) optimizer of the tensorflow-probability library. Note that we always randomly initialize the values for $\tau_1, \tau_2, \dots, \tau_{16}$ using the Glorot-Uniform initializer of the tensorflow-keras library, and implement the gradient tolerance of 10^{-8} .

References

1. Häffner, H. *et al.* Scalable multiparticle entanglement of trapped ions. *Nature* **438**, 643 (2005).
2. Hou, Z. *et al.* Full reconstruction of a 14-qubit state within four hours. *New J. Phys.* **18**, 083036, DOI: [10.1088/1367-2630/18/8/083036](https://doi.org/10.1088/1367-2630/18/8/083036) (2016).
3. Smolin, J. A., Gambetta, J. M. & Smith, G. Efficient Method for Computing the Maximum-Likelihood Quantum State from Measurements with Additive Gaussian Noise. *Phys. Rev. Lett.* **108**, 070502, DOI: [10.1103/PhysRevLett.108.070502](https://doi.org/10.1103/PhysRevLett.108.070502) (2012).
4. Lukens, J., Law, K., Jasra, A. & Lougovski, P. A practical and efficient approach for bayesian quantum state estimation. *New J. Phys.* (2020).
5. Teo, Y. S., Zhu, H., Englert, B.-G., Řeháček, J. & Hradil, Z. Quantum-state reconstruction by maximizing likelihood and entropy. *Phys. review letters* **107**, 020404 (2011).
6. James, D. F., Kwiat, P. G., Munro, W. J. & White, A. G. On the measurement of qubits. In *Asymptotic Theory of Quantum Statistical Inference: Selected Papers*, 509–538 (World Scientific, 2005).
7. Bolduc, E., Knee, G. C., Gauger, E. M. & Leach, J. Projected gradient descent algorithms for quantum state tomography. *npj Quantum Inf.* **3**, 1–9 (2017).
8. Qi, B. *et al.* Adaptive quantum state tomography via linear regression estimation: Theory and two-qubit experiment. *npj Quantum Inf.* **3**, 1–7 (2017).
9. Palmieri, A. M. *et al.* Experimental neural network enhanced quantum tomography. *npj Quantum Inf.* **6**, 1–5 (2020).
10. Torlai, G. *et al.* Neural-network quantum state tomography. *Nat. Phys.* **14**, 447–450 (2018).
11. Neugebauer, M. *et al.* Neural-network quantum state tomography in a two-qubit experiment. *Phys. Rev. A* **102**, 042604 (2020).
12. Ahmed, S., Muñoz, C. S., Nori, F. & Kockum, A. F. Quantum state tomography with conditional generative adversarial networks. *arXiv preprint arXiv:2008.03240* (2020).
13. Lohani, S., Kirby, B., Brodsky, M., Danaci, O. & Glasser, R. T. Machine learning assisted quantum state estimation. *Mach. Learn. Sci. Technol.* (2020).
14. Xu, Q. & Xu, S. Neural network state estimation for full quantum state tomography. *arXiv preprint arXiv:1811.06654* (2018).
15. Ahmed, S., Muñoz, C. S., Nori, F. & Kockum, A. F. Classification and reconstruction of optical quantum states with deep neural networks. *arXiv preprint arXiv:2012.02185* (2020).
16. Danaci, O., Lohani, S., Kirby, B. T. & Glasser, R. T. Machine learning pipeline for quantum state estimation with incomplete measurements. *arXiv preprint arXiv:2012.03104* (2020).
17. Abadi, M. *et al.* TensorFlow: Large-scale machine learning on heterogeneous systems (2015). Software available from tensorflow.org.
18. Higham, N. J. Analysis of the Cholesky Decomposition of a Semi-Definite Matrix. In *in Reliable Numerical Computation*, 161–185 (University Press, 1990).
19. Shende, V. V., Bullock, S. S. & Markov, I. L. Synthesis of quantum-logic circuits. *IEEE Transactions on Comput. Des. Integr. Circuits Syst.* **25**, 1000–1010 (2006).
20. Abraham, H. *et al.* Qiskit: An open-source framework for quantum computing, DOI: [10.5281/zenodo.2562110](https://doi.org/10.5281/zenodo.2562110) (2019).

Acknowledgements

This material is based upon work supported by, or in part by, the Army Research Laboratory and the Army Research Office under contract/grant numbers W911NF-19-2-0087 and W911NF-20-2-0168. The views and conclusions contained in this document are those of the authors and should not be interpreted as representing the official policies, either expressed or implied, of the Army Research Laboratory or the U.S. Government. The U.S. Government is authorized to reproduce and distribute reprints for Government purposes notwithstanding any copyright notation herein. T.A.S. acknowledges support from the IBM-HBCU Quantum Center and the Martin Luther King Visiting Scholars Program at MIT. Additionally, we acknowledge use of the IBM Q for this work. The views expressed are those of the authors and do not reflect the official policy or position of IBM Quantum. We would like to thank Joseph Lukens at Oak Ridge National Laboratory and Hanhee Paik at IBM for helpful discussions.

Author contributions statement

S.L. developed the setups, ran all simulations and measurements on IBM Q machine. S.L., B.T.K. and R.T.G. conceived of and led the project. All authors contributed to discussions and interpretations of the results, and wrote the manuscript.

Data availability

The data that support the findings of this study are available from the corresponding authors on reasonable request.

Competing interests

The authors declare no competing interests.

Supplementary

Supp.: Quantum circuits and tomography measurements

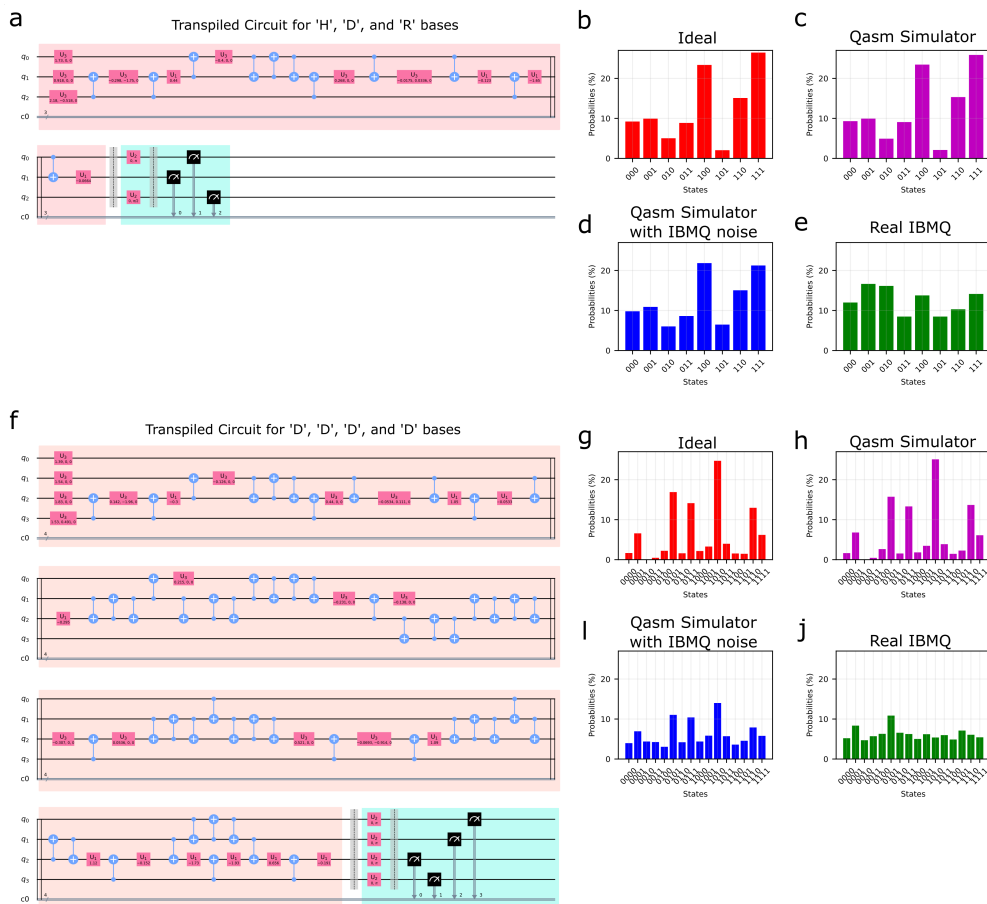


Figure S1. Examples of transpiled circuits for (a) three qubits, (f) four qubits, and corresponding probability measurements. (a, f) In the light-green box is the tomography portion of the circuit, while the preceding elements (light-red box), making up the bulk of the overall circuit, generate a random quantum state transpiled by the IBM Q backend ‘*ibmq_rome*’.

As mentioned in the manuscript, in order to perform the over-complete tomography for three qubits requires 27 quantum circuits, which increases to 81 for four qubits. Shown in Fig. S1 [a, f] is one example circuit for each of the three and four qubit cases, respectively. The light-green boxes in Fig. S1 [a, f] show the circuits’ tomography portion, while the remainder of the elements in the light-red boxes are the transpiled circuit used to generate random states. The corresponding projectors used to generate the probability amplitudes shown in Fig. S1 (b-e) and (g-j) are the result of measuring in the ‘H (first qubit)’, ‘D (second qubit)’, ‘R (third qubit)’ bases for three qubits and in the ‘D (first qubit)’, ‘D (second qubit)’, ‘D (third qubit)’, ‘D

(forth qubit)' for four qubits. For each measurement scenario we show the results for the ideal projection, ibmq-qasm simulator, ibmq-qasm simulator with IBMQ noise, and the real IBMQ computer.

Supp.: Reconstructing quantum states

The density matrices reconstructed directly from the network and the corresponding target density matrices are shown in Fig. S2. The network used is solely trained with the data obtained from the ideal tomography scenarios, whereas the test-set contains the tomography data obtained from the ideal mode, IBMQ qasm simulator with noise, and the real IBMQ computer.

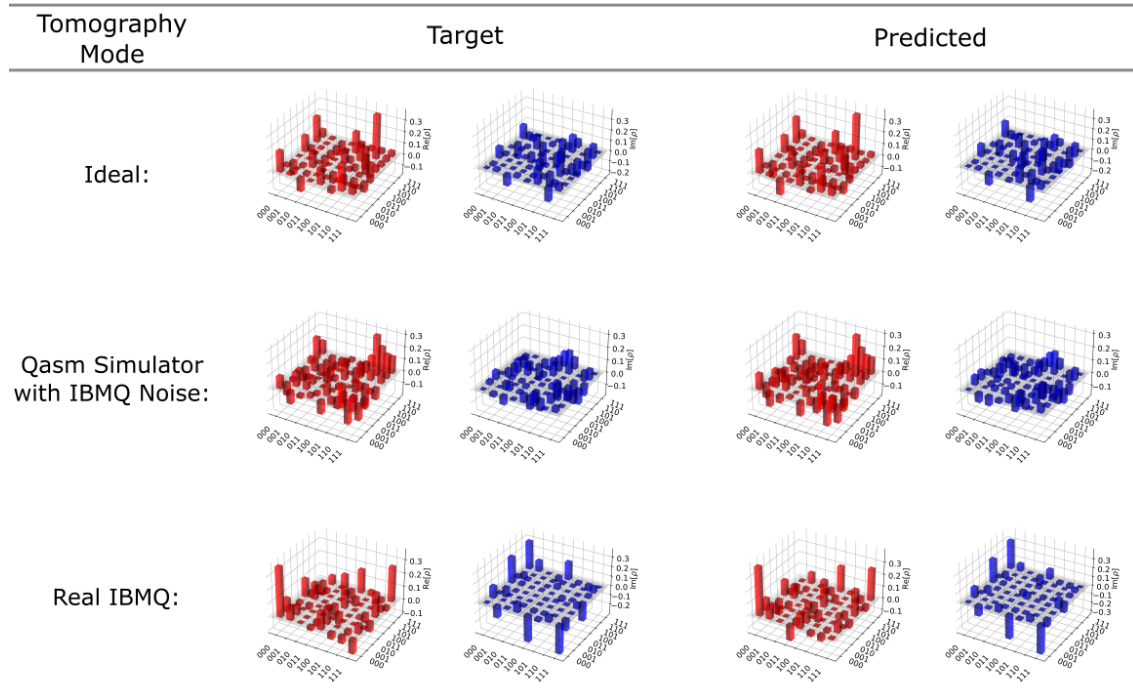


Figure S2. Examples of the target and predicted density matrices for tomography obtained from the ideal mode, IBMQ qasm simulator with noise, and the real IBMQ computer.